

Exploring the Association of Electron-Donating Corroles with Phthalocyanines as Electron Acceptors

Benedikt Platzer^{+, [a]}, Beatrice Berionni Berna^{+, [b, c]}, Martina Bischetti^[b], Daniel O. Cicero^[b], Roberto Paolesse^[b], Sara Nardis^{*, [b]}, Tomás Torres^{*, [c, d, e]} and Dirk M. Guldi^{*, [a]}

Abstract: Electron-donating corroles (Cor) were integrated with electron-accepting phthalocyanines (Pc) to afford two different non-covalent Cor·Pc systems. At the forefront was the coordination between a 10-meso-pyridine Cor and a ZnPc. The complexation was corroborated in a combination of NMR, absorption, and fluorescence assays, and revealed association with binding constants as high as 10^6 M^{-1} . Steady-state and time-resolved spectroscopies evidenced that re-

gardless of exciting Cor or Pc, the charge-separated state evolved efficiently in both cases, followed by a slow charge-recombination to reinstate the ground state. The introduction of non-covalent linkages between Cor and Pc induces sizeable differences in the context of light harvesting and transfer of charges when compared with covalently linked Cor-Pc conjugates.

Introduction

Photoinduced electron- and energy-transfer processes play a primary role in natural photosynthesis, which constitutes nature's way of converting light into usable chemical energy.^[1] More specifically, sunlight excites the natural antenna chromophores to provide electronic excitation, which is funneled to the reaction center by a cascade of electron and energy transfer

processes.^[2] The success of this process relies on the effectiveness of these electron transfers and the lack of recombination reactions that would interrupt the process and cause a waste of the absorbed energy.^[3] The fine structure-function-reactivity relationship that exists for naturally occurring photosynthetic reaction centers has prompted the design and the preparation of a variety of electron donor-acceptor ensembles, which have been developed and applied to many technologically relevant research fields, such as light-electricity conversion, light-fuel production, and optoelectronic devices.^[4]

Chlorophyll and bacteriochlorophylls, the most common of visible-light absorbing building blocks found in nature, are only one type of a more general subset of biologically inspired pigments composed, at their cores, of tetrapyrrolic macrocycles. Thus, porphyrinoids represent the natural choice in the design of multicomponent electron-donor-acceptor systems to mimic the natural reaction center as a replacement of the synthetically demanding and relatively unstable chlorophylls.^[5]

Corroles (Cor) and likewise phthalocyanines (Pc), have been extensively studied owing to their roles in mimicking biological systems.^[6] Their high thermal and chemical stability, their optical and redox properties,^[7] their tunability of these features by complexation with different metals or by different substitution at their peripheries render them excellent candidates for this purpose. Cor, with their maximum absorption in the range of 400–450 nm,^[8] together with the Pc maximum absorption centered at 600–700 nm,^[9] cover a large range of the solar spectrum, that is, from the UV to the near IR. Cor have widely been incorporated into multicomponent conjugates as electron donors due to their low oxidation potential, especially when compared with the porphyrin analogues.^[10] Pc have been proven to act as excellent electron acceptor counterparts, particularly when endowed with strong electron-withdrawing substituents.^[11]

Very recently, two conjugated panchromatic Cor-Pc conjugates have been reported.^[12] In both cases, the two differently

[a] B. Platzer,⁺ Prof. D. M. Guldi

Department of Chemistry and Pharmacy
Interdisciplinary Center for Molecular Materials (ICMM)
Friedrich-Alexander-Universität Erlangen-Nürnberg
Egerlandstr. 3, 91058 Erlangen (Germany)
E-mail: dirk.guldi@fau.de

[b] Dr. B. Berionni Berna,⁺ Dr. M. Bischetti, Prof. D. O. Cicero, Prof. R. Paolesse, Prof. S. Nardis

Department of Chemical Science and Technologies
University of Rome Tor Vergata
Via della Ricerca Scientifica, 00133 Rome (Italy)
E-mail: nardis@scienze.uniroma2.it

[c] Dr. B. Berionni Berna,⁺ Prof. T. Torres

Departamento de Química Orgánica
Universidad Autónoma de Madrid, Campus de Cantoblanco
C/ Francisco Tomás y Valiente 7, 28049 Madrid (Spain)
E-mail: tomas.torres@uam.es

[d] Prof. T. Torres

Institute for Advanced Research in Chemical Sciences (IAdChem)
Universidad Autónoma de Madrid, Campus de Cantoblanco, 28049 Madrid (Spain)

[e] Prof. T. Torres

IMDEA-Nanociencia,
C/Faraday 9, Campus de Cantoblanco, 28049 Madrid (Spain)

[⁺] These authors contributed equally to this manuscript.

Supporting information for this article is available on the WWW under <https://doi.org/10.1002/chem.202103891>

© 2022 The Authors. Chemistry - A European Journal published by Wiley-VCH GmbH. This is an open access article under the terms of the Creative Commons Attribution License, which permits use, distribution and reproduction in any medium, provided the original work is properly cited.

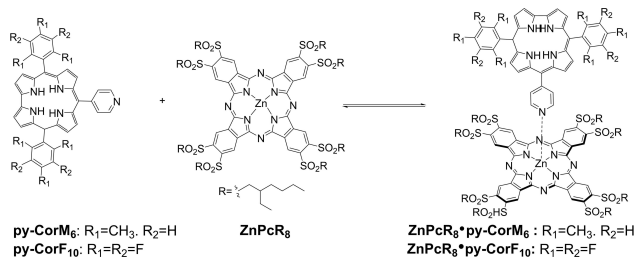
substituted Cor operate as primary electron donors after photoexcitation, while the conjugated electron accepting Pc functions as primary electron acceptor.

It is noteworthy that in the natural systems the light harvesters of the antennas as well as the electron donors and electron acceptors in the reaction centers are brought together through non-covalent interactions. Compared with artificial light-transforming systems, in which covalent linkages are employed, light-harvesting systems based on non-covalent interactions undoubtedly present several benefits. First, they are easier to fabricate without the needs of multiple synthetic steps. Second, the solution stability is tunable by the careful choice of the supramolecular interactions and/or the external stimuli. Third, the control over the assembly/disassembly of such supramolecular systems does allow perturbing and modulating some of their physicochemical properties. Among the many different non-covalent interactions, metal-ligand coordination is an efficient means to self-assemble Cor- and Pc-based electron donor-acceptor ensembles.^[13]

In the current study, two different Cor, bearing substituents with drastically different electronic behaviour in their 5 and 15 *meso*-positions were prepared and connected to an electron accepting ZnPc by metal-ligand, axial coordination of pyridyl in the 10 *meso*-position of Cor to zinc metal center of Pc (Scheme 1).

Results and Discussion

A widely extended method to obtain *trans*-A₂B Cor relies on the reaction of the desired dipyrromethane with a suitable aldehyde.^[14] Starting from mesitylbenzaldehyde for the synthesis of **py-CorM₆** and pentafluorobenzaldehyde for the synthesis of **py-CorF₁₀**, the corresponding dipyrromethanes were synthesized by a reaction with pyrrole, using the method already reported in the literature.^[15] Both 10-*meso*-pyridyl-substituted Cor were obtained following an already reported procedure, aimed to the synthesis of *trans*-A₂B-corroles bearing substituents with basic nitrogen atoms at the *meso*-positions. Cor formation reaction involves the acid-catalyzed condensation of a dipyrromethane with an aldehyde followed by oxidation with DDQ.^[16] Octakis(2-ethylhexylsulfonyl) Zn(II)Pc (**ZnPcR₈**) was prepared as already reported in the literature.^[11b]



Scheme 1. Metal-ligand, axial coordination of either **py-CorM₆** or **py-CorF₁₀** with **ZnPcR₈** to afford **ZnPcR₈·py-CorM₆** and **ZnPcR₈·py-CorF₁₀**.

NMR titrations

Measurements were carried out in CDCl₃ at 20 °C with a constant concentration of **py-CorM₆** (100 μM) and variable concentrations of **ZnPcR₈**. To appreciate changes in the chemical shifts a complete assignment of **py-CorM₆** and **ZnPcR₈·py-CorM₆** was necessary. The assigned ¹H NMR spectrum of **py-CorM₆** is shown in Figure 1. Methyl resonances were assigned based on their different integration values in the aliphatic range from 1.98 and 2.66 ppm. Assignment of the protons in the β-pyrrolic positions were done by combining the COSY and ROESY spectra. Protons at positions 2 and 18 were unambiguously found at 8.95 ppm. These protons are not subject to any dipolar interactions with CH₃ *ortho*-functionalities of the *meso*-phenyl groups as they do not feature any cross peaks in the ROESY analyses (Figure 2). Any other assignment of, for example, the aromatic protons was possible by the combination of COSY and ROESY. Figure 3 shows the scalar

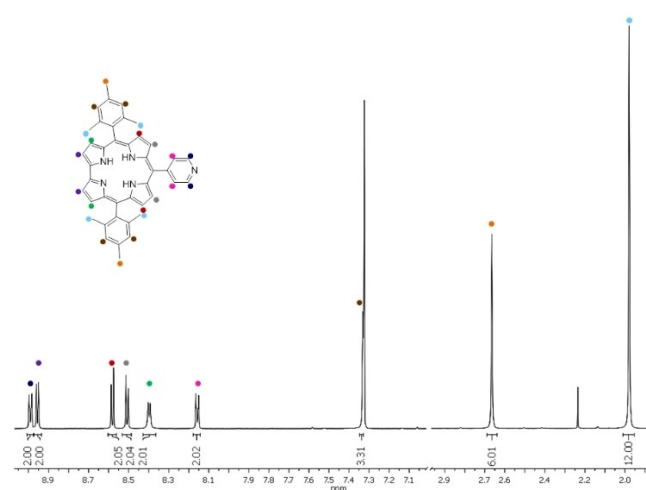


Figure 1. ¹H NMR spectrum of **py-CorM₆** in CDCl₃ at room temperature. Full assignment obtained after combining COSY, ROESY, and ¹H-¹³C HSQC techniques.

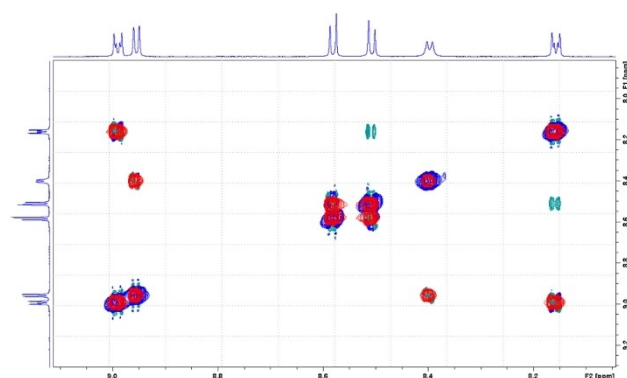


Figure 2. Combination of COSY (red) and ROESY (green and blue) analyses of **py-CorM₆** in CDCl₃ at room temperature (focus on the *meso*-pyridine and β-pyrrolic signals). Green cross peaks indicate a dipolar correlation of protons at position 8 and 12 with the two *ortho*-pyridine protons.

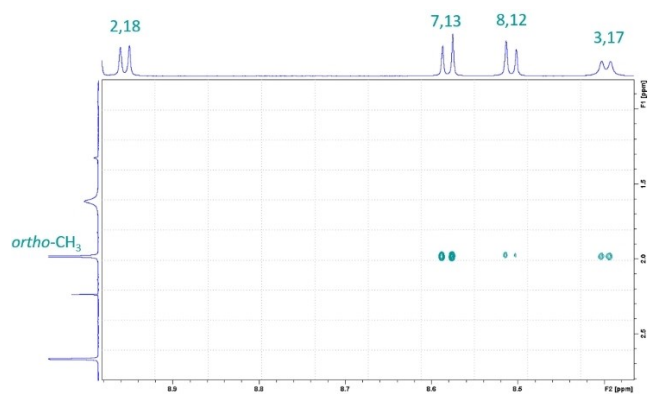


Figure 3. ROESY spectrum of the β -pyrrolic positions of **py-CorM₆** in CDCl_3 at room temperature. Protons at positions 2 and 18 lack any cross peak with the CH_3 *ortho*-functionalities of the *meso*-phenyl groups.

couplings between the protons in the positions 2,18 and 3,17, and a cross-peak due to a dipolar correlation of the 8,12 β -pyrrolic protons with the two pyridine protons.

A typical titration of **py-CorM₆** with **ZnPcR₈** is summarized in Figure 4. Upon addition of **ZnPcR₈** a severe broadening of the peak line-widths is observed, which renders the assignment of some protons rather difficult. Still, all peaks shift toward lower ppm with, however, different magnitudes. Changes become discernable at 0.25 equivalents of **ZnPcR₈** and the pyridine protons, which are the closest to **ZnPcR₈**, are those that are most affected by the aromatic ring current. To appreciate the $\Delta\delta$ from Cor, 2-dimensional analyses of **ZnPcR₈·py-CorM₆** were performed using the same concentration for both of them, that is, 2.5 mM (Figures S4–7). The initial and the final step of the titration experiments are shown in Figure 5 next to the chemical shift perturbations experienced by **py-CorM₆**. Following the **ZnPcR₈·py-CorM₆** formation, the

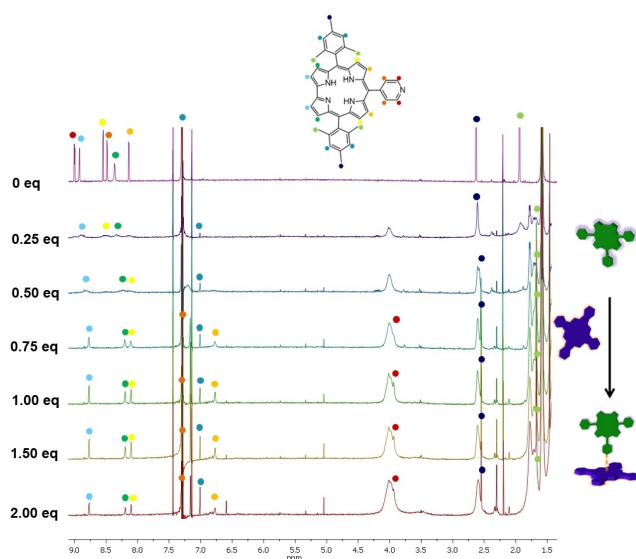


Figure 4. ^1H NMR titration assays of **py-CorM₆** with variable equivalents of **ZnPcR₈** in CDCl_3 at 20°C .

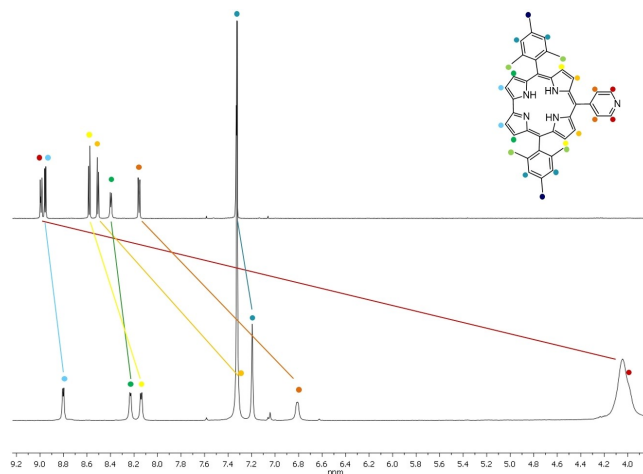


Figure 5. First (0 equiv. of **ZnPcR₈**) and last (2 equiv. **ZnPcR₈**) ^1H NMR spectra of the titrations performed with **py-CorM₆** and **ZnPcR₈**. Inset displays a table with the chemical shift perturbations of the **py-CorM₆** protons.

chemical shift perturbation varies from about 0.08 all the way to 5.01 ppm.

From these experiments it is, however, evident that the concentrations were too high to determine the effective thermodynamic constant K_D . In particular, the range of $[\text{Pc}]/[\text{Corr}]$ was insufficient to cover the full curvature of the binding plot. As such, the signals seem to saturate already at 0.75 equivalents of Pc, which makes the value of the binding constant unreliable.

At, for example, $100\ \mu\text{M}$ of **py-CorM₆**, the association constant is predicted to be greater or equal to $10^6\ \text{M}^{-1}$. Overall, we feel that it represents a useful estimate for the exchange constant, k_{exc} .

The different $\Delta\delta$ values, which are tabled in the inset of Figure 5, stem from different exchange regimes that the Cor protons experience. Aliphatic mesityl protons (dark blue and light green dots in Figure 4) are barely affected by the electronic changes due to complexation. This results in a fast exchange, in which the peak intensities remain constant throughout the titrations. Protons belonging to the pyridine moiety and to the positions 7,13 and 8,12 of the corrole macrocycle (red, orange, light orange, and yellow dots in Figure 4) are the most affected by the interaction, and display a slow exchange behavior. Protons in the Cor 2,18, 3,17 positions, as well as the aromatic protons of the mesityl groups, which are marked in light blue, green, and blue in Figure 4, are affected by an intermediate exchange regime. Here, the resonance lines become very broad as the Pc is added and the system slowly equilibrates from the free macrocycle to the fully coordinated Pc-Corr. As such, we gather information about how to estimate k_{exc} from the aromatic protons belonging to the mesityl group: prior to any **ZnPcR₈** addition, their signal was covered by the solvent (Figure 5). Throughout the titration experiments, a shift toward lower ppm was evident and the intensities of the new peaks directly relate to the concentration of **ZnPcR₈·py-CorM₆**. In the case of intermediate exchange conditions, k_{exc} is

approximated by taking the differences of chemical shifts between the free and bound corrole. The chemical shift perturbation was found to be 0.148 ppm, resulting in an exchange rate value of $k_{\text{exc}} \approx 103 \text{ s}^{-1}$.

To assist in the interpretation of the NMR data and to gather more quantitative information about the binding phenomenon, different sets of physicochemical experiments were performed. To elucidate the electronic behaviour of Cor and its function as light harvester and electron donor to power energy and/or electron transfer upon photoexcitation, we complemented our investigation by probing **py-CorF₁₀**.

Electrochemical characterization

Square-wave and cyclic voltammograms of **py-CorM₆** and **py-CorF₁₀** next to **ZnPcR₈** were recorded in dichloromethane with 0.1 M [Bu₄N][PF₆] as electrolyte (Figures S8–10). **py-CorM₆** and **py-CorF₁₀** both feature single reductions and oxidations, which are *quasi* reversible and reversible, respectively, at -1.85 and $+0.34$ V versus Fc/Fc⁺ for **py-CorM₆** as well as at -1.58 and $+0.58$ V versus Fc/Fc⁺ for **py-CorF₁₀**. Importantly, **py-CorF₁₀** is by far a better electron acceptor and a poorer electron donor than **py-CorM₆**, due to the electron-withdrawing substituents. In contrast, four reductions and a single oxidation are seen for **ZnPcR₈**, that is, at -0.74 , -0.99 , -1.09 , and -1.30 V versus Fc/Fc⁺ as well as at $+0.90$ V versus Fc/Fc⁺. All **ZnPcR₈**-based values, with the exception of the second reduction, are in agreement with those determined for a ZnPc-reference.^[10b] Reductions and oxidations are summarised in Table 1. Combining **py-CorM₆** and **py-CorF₁₀** as electron donors and **ZnPcR₈** as electron acceptor, respectively, and realizing **ZnPcR₈·py-CorM₆** and **ZnPcR₈·py-CorF₁₀** results into charge-separated state energies of 1.08 and 1.32 eV, respectively.

Spectro-electrochemical experiments were conducted for **py-CorM₆** and **py-CorF₁₀** in dichloromethane, while *o*-dichlorobenzene turned out to be better suited for **ZnPcR₈** (Figure 6). **py-CorM₆** and **py-CorF₁₀** feature similar differential spectra upon their one-electron oxidations with 370–390, 445, 625, and 670 nm maxima, as well as 410, 425, 565, and 600–605 nm minima. **ZnPcR₈** reveals upon its one-electron reduction maxima at 430, 600, 640, 705, and 770 nm, while minima are seen at 380, 620, 660, and 690 nm. In the near infrared, the maxima are at 960 and 1095 nm.

Table 1. Reductions and oxidations of **py-CorM₆**, **py-CorF₁₀**, and **ZnPcR₈** in V vs. Fc/Fc⁺ with 0.1 M [Bu₄N][PF₆] as electrolyte.

| | 4th red. | 3rd red. | 2nd red. | 1st red. | 1st ox. |
|-----------------------------|----------|----------|----------|----------|---------|
| py-CorM₆ | | | | -1.85 | $+0.34$ |
| py-CorF₁₀ | | | | -1.58 | $+0.58$ |
| ZnPcR₈ | -1.30 | -1.09 | -0.99 | -0.74 | $+0.90$ |

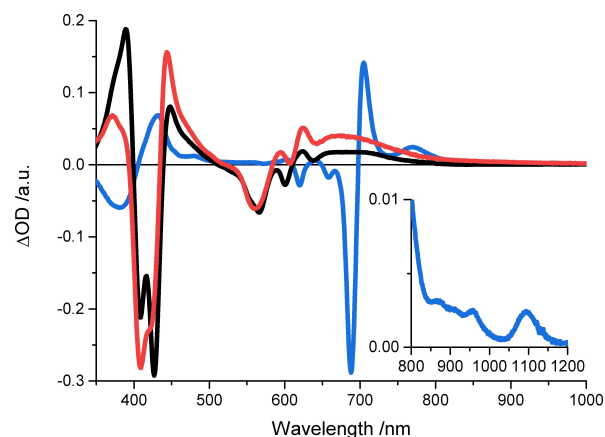


Figure 6. Differential absorption spectra obtained upon one-electron oxidation of **py-CorM₆** (black) and **py-CorF₁₀** (red) at a bias of $+0.9$ V vs. Ag-wire in de-aerated dichloromethane with 0.1 M [Bu₄N][PF₆] as electrolyte and upon one-electron reduction of **ZnPcR₈** (blue) at a bias of -0.8 V vs. Ag-wire in de-aerated *o*-dichlorobenzene with 0.1 M [Bu₄N][ClO₄] as electrolyte.

Photophysical characterization

Steady-state absorption and fluorescence spectra of **py-CorM₆**, **py-CorF₁₀**, and **ZnPcR₈** were recorded in toluene (Figure 7).

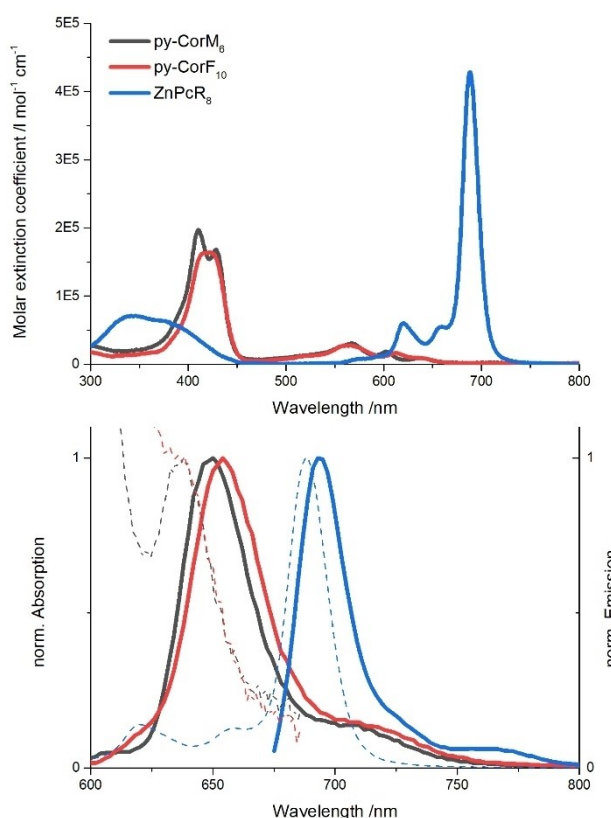


Figure 7. Absorption spectra at the top and normalized fluorescence spectra at the bottom of **py-CorM₆** (black), **py-CorF₁₀** (red), and **ZnPcR₈** (blue) in toluene at room-temperature including the corresponding absorption spectra (dashed lines).

Hereby, the absorption spectra of **py-CorM₆** and **py-CorF₁₀** are dominated by two strong Soret-band absorptions at 410/429 and 415/424 nm, respectively.

In each case, four weak Q-band absorptions evolve in the range from 510 to 640 nm. **ZnPcR₈** features weak Soret-band absorptions in the 320 to 400 nm range and a multitude of strong Q-band absorptions, which peak at 688 nm. The latter complement those of **py-CorM₆** and **py-CorF₁₀**. When turning to the fluorescence spectra, the respective maxima are 650 nm (**py-CorM₆**), 654 nm (**py-CorF₁₀**), and 694 nm (**ZnPcR₈**). They exhibit nearly the same energies and quantum yields. In particular, the quantum yields are 0.29, 0.19, and 0.29 for **py-CorM₆**, **py-CorF₁₀**, and **ZnPcR₈**, respectively. All relevant values are summarised in Table 2.

Formation of **ZnPcR₈·py-CorM₆** and **ZnPcR₈·py-CorF₁₀** was followed and analyzed in steady-state absorption and fluorescence assays. Variable concentrations of either **py-CorM₆** or **py-CorF₁₀** were added to a solution of **ZnPcR₈**, whose concentration was kept constant. Throughout these titrations the **ZnPcR₈**-centered Q-band absorption at 688 nm red-shifts and attenuates. Hand-in-hand with the red-shifted absorption is a **ZnPcR₈**-centered fluorescence that is subject to a non-linear quenching. In this regard, the association constants are $1.8 \pm 0.2 \times 10^6 \text{ M}^{-1}$ for **ZnPcR₈·py-CorM₆** as well as $6.0 \pm 1.1 \times 10^5 \text{ M}^{-1}$ for **ZnPcR₈·py-CorF₁₀** (Figures 8 & S11). Employing chlorobenzene led like toluene to appreciable changes with comparable constants on the order of 10^6 M^{-1} (Figures S14 & S15).

Measurements with a Cor-reference resulted in a similar non-linear fluorescence quenching. Even the association constant is in the same range, that is, $2.8 \pm 0.7 \times 10^6 \text{ M}^{-1}$ and is, thus, consistent with the NMR data (Figure S16). When using a ZnPc-reference, which features *tert*-butyl groups, the fluorescence quenching was much weaker (Figures S18 & S19). The association constants are $2.7 \pm 1.1 \times 10^5$ and $1.4 \pm 0.3 \times 10^5 \text{ M}^{-1}$ for **ZnPc·py-CorM₆** and **ZnPc·py-CorF₁₀**, respectively. Titrations in anisole and ethanol led to significantly weaker binding with association constants in the range of 10^4 M^{-1} rather than 10^5 or 10^6 M^{-1} (Figures S12, S13 & S17).

Finally, temperature-dependent titration experiments were performed with mixtures of **py-CorM₆**, **py-CorF₁₀**, and Cor-reference as well as **ZnPcR₈** in toluene in the range from 20 to 60 °C (Figures S20–22). Overall, the association constants decreased as the temperatures were increased. This is well in line with the notion that the formation of **ZnPcR₈·py-CorM₆** and **ZnPcR₈·py-CorF₁₀** is exergonic. Increasing the temperature is also associated with a slightly weaker fluorescence quenching. This prompts to a slower, but still exergonic separation of

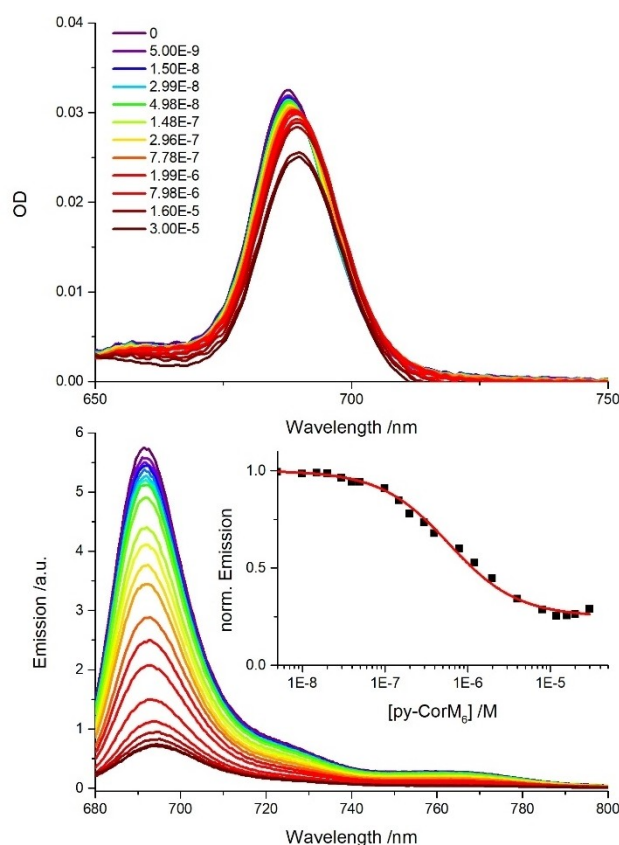


Figure 8. Absorption spectra at the top and fluorescence spectra at the bottom of **ZnPcR₈** ($1 \times 10^{-7} \text{ M}$) upon addition of variable **py-CorM₆** concentrations ($0\text{--}3 \times 10^{-5} \text{ M}$) in toluene at room-temperature. Inset displays the normalized **ZnPcR₈** fluorescence to determine the binding constant.

charges, while the intrinsic **ZnPcR₈** fluorescence remains unaffected.

Insights into the excited state dynamics were gathered by photo-exciting **py-CorM₆/py-CorF₁₀** and **ZnPcR₈** at 430 and 676 nm, respectively. In the case of **py-CorM₆**, the first three transient species feature characteristics of the singlet excited state. These were maxima at 460 and 800 nm next to minima at 568 and 604 nm (Figure S23). The first two relaxations take place with 3 and 47 ps and transform the initially vibrationally and electronically hot singlet excited state into the fully relaxed and fluorescent singlet excited state. The latter transforms ultimately into the triplet excited state with its red-shifted 455 nm maximum. The singlet excited state of **py-CorF₁₀** features a minimum at 565 nm and maxima at 460, 750 and $< 1250 \text{ nm}$. Initially, it is the vibrationally and electronically hot singlet excited state that is formed. It relaxes with 24 ps before it decays into the triplet excited state, for which the latter two maxima are missing, within several ns (Figure S24). For **ZnPcR₈**, a vibrationally and electronically hot singlet excited state relaxes with 14 and 555 ps to afford a relaxed singlet excited state. Signatures of the latter are maxima at 510 and 887 nm as well as a ground state bleaching at 695 nm. The corresponding triplet excited state with maxima at 440 and 795 nm and

Table 2. Absorption maxima, molar extinction coefficients ϵ_{max} , fluorescence maxima, and fluorescence quantum yields Φ_{Fl} in toluene. Tetraphenylporphyrin (**H₂TPP**) and zinc tetra-*tert*-butyl-phthalocyanine (**ZnTtBuPc**) were used as the respective references for Cor and ZnPc.^[17]

| | Absorption _{max} | $\epsilon_{\text{max}}/\text{cm}^{-1} \text{ M}^{-1}$ | Fluorescence _{max} | Φ_{Fl} |
|-----------------------------|---------------------------|---|-----------------------------|--------------------|
| py-CorM₆ | 410 nm | 1.97×10^5 | 650 nm | 0.29 |
| py-CorF₁₀ | 424 nm | 1.64×10^5 | 654 nm | 0.19 |
| ZnPcR₈ | 688 nm | 4.28×10^5 | 694 nm | 0.29 |

ground state bleaching at 692 nm (Figure S25) is formed with 2.3 ns before it decays to the ground state.

Mixtures of **py-CorM₆** and **ZnPcR₈** as well as **py-CorF₁₀** and **ZnPcR₈** were probed by means of 430 and 676/670 nm photo-excitation experiments, respectively. Using an excess of **ZnPcR₈**, implies the 676/670 nm co-excitation of either **ZnPcR₈·py-CorM₆** or **ZnPcR₈·py-CorF₁₀**, on one hand, and **ZnPcR₈**, on the other hand. In such a case, a model with a total of four species was fully sufficient to fit the raw data. Two of them relate to **ZnPcR₈·py-CorM₆/ZnPcR₈·py-CorF₁₀** and the other two to **ZnPcR₈**. As a leading example, 676 nm photo-excitation of **ZnPcR₈·py-CorM₆** leads in toluene to the **ZnPcR₈**-centered singlet excited state formation (Figure 9). It decays with 5 ps and yields in 77% a charge separated state, that is, **[ZnPcR₈]^{•-}·[py-CorM₆]^{•+}**. Evidence for the charge separation comes

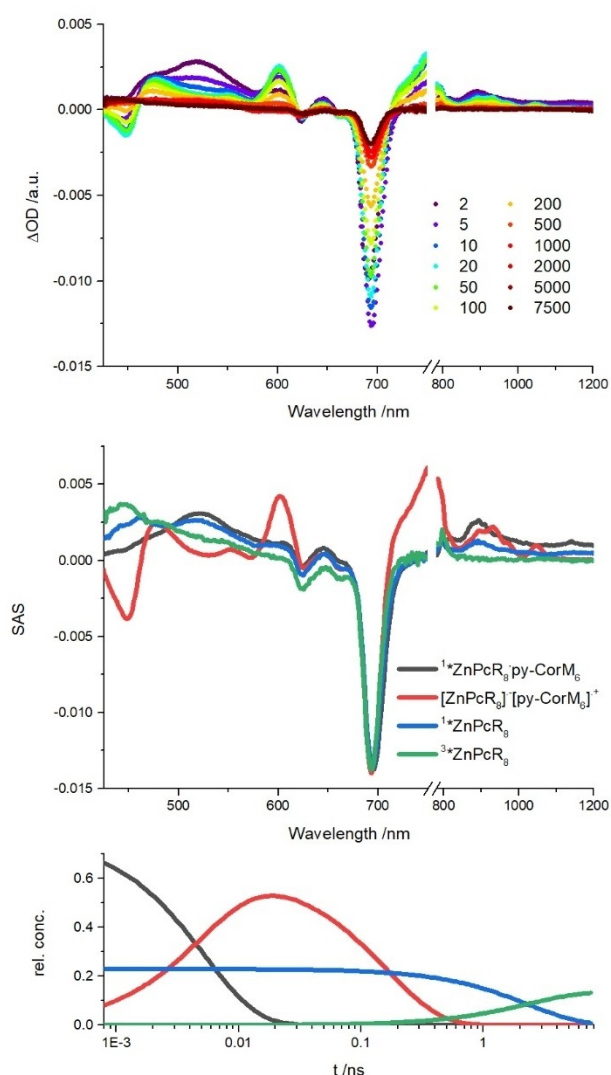


Figure 9. Differential absorption spectra on the top obtained upon femto-second flash-photolysis (676 nm) of a 10:1 mixture of **py-CorM₆** and **ZnPcR₈** in de-aerated toluene at room-temperature with time delays between 2 and 7500 ps. Species associated spectra of **1*ZnPcR₈·py-CorM₆** (black), **[ZnPcR₈]^{•-}·[py-CorM₆]^{•+}** (red), **1*ZnPcR₈** (blue), and **3*ZnPcR₈** (green) in the center and relative concentration profiles of the transient species at the bottom.

from the observation of the one-electron reduced form of **ZnPcR₈** with maxima at 600, 750–780, 935, 970, and 1050 nm and of the electron oxidized form of **py-CorM₆** with a ground state bleaching and a maximum at 450 and 480 nm, respectively. It reinstates the ground state with 164 ps. Meanwhile non-complexed **ZnPcR₈** undergoes intersystem crossing, by which the singlet excited state interconverts into the triplet excited state with 2.3 ns. Similar results are obtained for **ZnPcR₈·py-CorF₁₀** with lifetimes of 12 and 1400 ps for the singlet excited state and the **[ZnPcR₈]^{•-}·[py-CorF₁₀]^{•+}** charge separated state, respectively (Figure S26). Corresponding experiments in anisole are virtually identical. Upon photo-excitation at 670 nm, 6 and 11 ps are the **ZnPcR₈**-centered singlet excited state lifetimes in **ZnPcR₈·py-CorM₆** and **ZnPcR₈·py-CorF₁₀**, respectively. The corresponding charge-separated states are formed in 84% for **[ZnPcR₈]^{•-}·[py-CorM₆]^{•+}** and 94% for **[ZnPcR₈]^{•-}·[py-CorF₁₀]^{•+}**. The decays are 29 and 127 ps as the ground-states are recovered (Figures S29–30). All relevant lifetimes are put together in Table 3. Charge separation was also successful with 75% yield upon photoexcitation at 430 nm in the presence of an excess of **ZnPcR₈**. In these cases, the starting point was, however, mostly **py-CorM₆·py-CorF₁₀**-centered (Figures S27–28).

Conclusion

We have explored supramolecular interactions between two different corroles (Cor) bearing either electron-donating or electron-withdrawing groups, with an electron-withdrawing-substituted phthalocyanine (Pc). Strong chemical-shift perturbations were observed in ¹H NMR analyses of titrations, up to 5 ppm. Qualitative information regarding the binding constant and exchange constant was gathered. To assist the interpretation of the NMR data, excited-state properties were studied. Photoexcitation of either the Pc or Cor is the starting point to a fast charge-separation in combination with a slow charge-recombination. The latter reaches well into the thousands of picoseconds. Importantly, even if perfluorinated, Cor proves to be an excellent electron donor, highlighting its utility as sensitizer in light-harvesting applications.

Experimental Section

Material and general methods: Unless otherwise stated, all reagents and solvents were obtained from commercial suppliers and used without further purification. Chromatography: Thin layer chromatography (TLC) analyses were performed on aluminum sheets coated with silica gel 60 F254 or neutral alumina 60 F254 (Merck). TLC analyses were carried out with an UV lamp of 254 and

Table 3. Charge separation and recombination for **ZnPcR₈·py-CorM₆** and **ZnPcR₈·py-CorF₁₀** in toluene and anisole.

| | ZnPcR ₈ ·py-CorM ₆ | | ZnPcR ₈ ·py-CorF ₁₀ | |
|---------|--|--------|---|---------|
| toluene | 5 ps | 164 ps | 12 ps | 1400 ps |
| anisole | 6 ps | 29 ps | 11 ps | 127 ps |

365 nm. Column chromatography was carried out using silica gel Merck-60 (230–400 mesh, 60 Å), Sigma-Aldrich (70–230 mesh, 60 Å) and neutral alumina (Merk, Brockmann Grade III) as the solid support. Eluents and relative proportions are indicated for each particular case. Nuclear magnetic resonance (NMR): for structural assignments ^1H and ^{13}C spectra were recorded on a Bruker Avance spectrometer operating at 700 MHz for ^1H , equipped with a 5 mm inverse TXI probe and z-axis gradients. Chemical shifts are reported on the δ scale (ppm), where the residual solvent signal has been used as an internal reference. The NMR spectra were processed using the software MestreNova 11.0.

Electrochemistry: Square-wave and cyclic voltammetry were performed on a three-electrode setup (WE: C, CE: Pt, RE: Ag) with Fc^+ as an internal standard. Solvents were de-aerated using Ar. **Spectroelectrochemistry:** A three electrode-setup (WE: Pt-mesh, CE: Pt, RE: Ag) was used together with a custom-made glass cell. Absorption was measured through the transparent WE with an Agilent CARY 5000 UV-Vis-NIR spectrophotometer. Solvents were de-aerated using Ar. **Steady-state Absorption & Fluorescence:** 10x10 mm quartz cuvettes were used for both methods. Absorption was measured at a Perkin Elmer Lambda 2 spectrometer, a Horiba Jobin Yvon Fluoromax 3 was used for Fluorescence experiments.

Transient absorption: Spectra were obtained with a Ti:sapphire laser system CPA-2101 (Clark-MXR, Inc.) paired with an Ultrafast Inc. Helios TAPPS-transient absorption pump probe spectroscopy detection unit (pump: 1 kHz repetition, 150 fs pulse width). 2x10 mm quartz cells were used while spectra were acquired with an Ultrafast Systems HELIOS transient absorption spectrometer.

Synthetic procedures: Py-CorF_{10} , $\text{py-CorM}_6^{[15-16]}$ and $\text{ZnPcR}_8^{[11b]}$ were prepared following literature procedures.

Acknowledgements

This work was supported by the Spanish MINECO, PID2020-116490GB-I00 (Porphyrinoids, T.T) and by the Italian PRIN MIUR “SUNSET” 2017EKCS35_002. IMDEA-Nanociencia also acknowledges support from the “Severo Ochoa” Programme for Centres of Excellence in R&D (MINECO, Grant SEV-2016-0686). Open Access funding enabled and organized by Projekt DEAL.

Conflict of Interest

The authors declare no conflict of interest.

Keywords: electron transfer • organic photovoltaics • porphyrinoids • supramolecular chemistry

- [1] a) B. Alberts, B. Alberts, A. Johnson, J. Lewis, M. C. Raff, K. Roberts, P. Walter, J. H. Wilson, T. Hunt, *Molecular Biology of the Cell*, Garland Science, New York, 2008; b) D. K. Dogutan, D. G. Nocera, *Acc. Chem. Res.* **2019**, 52, 3143.
- [2] K. Kato, T. Shinoda, R. Nagao, S. Akimoto, T. Suzuki, N. Dohmae, M. Chen, S. I. Allakhverdiev, J. R. Shen, F. Akita, N. Miyazaki, T. Tomo, *Nat. Commun.* **2020**, 11, 238.
- [3] a) V. Balzani, A. Credi, M. Venturi, *ChemSusChem* **2008**, 1, 26; b) R. E. Blankenship, *Molecular Mechanisms of Photosynthesis*, 2nd Edition, John Wiley & Sons, 2014; c) B. R. Green, W. W. Parson, *Light-harvesting*

- antennas in photosynthesis*, Springer, Dordrecht, London **2011**; d) N. Nelson, C. F. Yocum, *Annu. Rev. Plant Biol.* **2006**, 57, 521; e) J. H. Wilson, T. Hunt, *Molecular biology of the cell, 4th edition : a problems approach*, Garland Science, New York, London **2002**.
- [4] a) M. Hao, G. Sun, M. Zuo, Z. Xu, Y. Chen, X.-Y. Hu, L. Wang, *Angew. Chem. Int. Ed.* **2020**, 59, 10095; *Angew. Chem.* **2020**, 132, 10181; b) G. Sun, M. Zuo, W. Qian, J. Jiao, X.-Y. Hu, L. Wang, *Green Synth. Catal.* **2021**, 2, 32; c) Z. Zhang, Z. Zhao, Y. Hou, H. Wang, X. Li, G. He, M. Zhang, *Angew. Chem. Int. Ed.* **2019**, 58, 8862; *Angew. Chem.* **2019**, 131, 8954; d) Y. Tao, C. Yang, J. Qin, *Chem. Soc. Rev.* **2011**, 40, 2943; e) S.-C. Lo, P. L. Burn, *Chem. Rev.* **2007**, 107, 1097; f) S. Saha, J. F. Stoddart, *Chem. Soc. Rev.* **2007**, 36, 77; g) H. Q. Peng, L. Y. Niu, Y. Z. Chen, L. Z. Wu, C. H. Tung, Q. Z. Yang, *Chem. Rev.* **2015**, 115, 7502; h) J. M. Yuen, J. R. Diers, E. J. Alexy, A. Roy, A. K. Mandal, H. S. Kang, D. M. Niedzwiedzki, C. Kirmaier, J. S. Lindsey, D. F. Bocian, D. Holten, *J. Phys. Chem. A* **2018**, 122, 7181; i) A. Agresti, B. Berionni Berna, S. Pescetelli, A. Catini, F. Menchini, C. Di Natale, R. Paolesse, A. Di Carlo, *Adv. Funct. Mater.* **2020**, 30, 2003790; j) D. Guzmán, I. Papadopoulos, G. Lavarda, P. R. Rami, R. R. Tykwinski, M. S. Rodríguez-Morgade, D. M. Guldi, T. Torres, *Angew. Chem. Int. Ed.* **2021**, 60, 1474; *Angew. Chem.* **2021**, 133, 1496.
- [5] D. Gust, T. Moore, A. L. Moore, *Acc. Chem. Res.* **1993**, 26, 198.
- [6] a) D. Wróbel, *Mol. Cryst. Liq. Cryst.* **2016**, 627, 4; b) G. Bottari, G. de la Torre, D. M. Guldi, T. Torres, *Coord. Chem. Rev.* **2021**, 428, 213605; c) Z.-W. Li, J.-J. Yang, X.-Y. Liu, W.-H. Fang, H. Wang, G. Cui, *Chem. Eur. J.* **2021**, 27, 4159; d) E. Anaya-Plaza, J. Joseph, S. Baurath, M. Wagner, C. Dolle, M. Sekita, F. Gröhn, E. Spiecker, T. Clark, A. de la Escosura, D. M. Guldi, T. Torres, *Angew. Chem. Int. Ed.* **2020**, 59, 18786; *Angew. Chem.* **2020**, 132, 18946; e) M. Urbani, M.-E. Ragoussi, M. K. Nazeeruddin, T. Torres, *Coord. Chem. Rev.* **2019**, 381, 1.
- [7] a) A. Ghosh, *Chem. Rev.* **2017**, 117, 3798; b) G. de la Torre, C. G. Claessens, T. Torres, *Chem. Commun.* **2007**, 2000; c) D. Wöhrle, *Adv. Mater.* **1993**, 5, 942.
- [8] a) R. Paolesse, A. Marini, S. Nardis, A. Froio, F. Mandoj, D. J. Nurco, L. Prodi, M. Montalti, K. M. Smith, *J. Porphyrins Phthalocyanines* **2003**, 07, 25; b) B. Ventura, A. Degli Esposti, B. Kozarna, D. T. Gryko, L. Flamigni, *New J. Chem.* **2005**, 29, 1559; c) T. Ding, E. A. Alemán, D. A. Modarelli, C. J. Ziegler, *J. Phys. Chem. A* **2005**, 109, 7411.
- [9] a) N. Kobayashi, H. Ogata, N. Nonaka, E. A. Luk'yanets, *Chem. Eur. J.* **2003**, 9, 5123; b) D. Chahraoui, P. Valat, J. Kossanyi, *Res. Chem. Intermed.* **1992**, 17, 219.
- [10] a) Y. Fang, Z. Ou, K. M. Kadish, *Chem. Rev.* **2017**, 117, 3377; b) L. Flamigni, D. T. Gryko, *Chem. Soc. Rev.* **2009**, 38, 1635.
- [11] a) A. R. M. Soares, M. V. Martínez-Díaz, A. Bruckner, A. M. V. M. Pereira, J. P. C. Tomé, C. M. A. Alonso, M. A. F. Faustino, M. G. P. M. S. Neves, A. C. Tomé, A. M. S. Silva, J. A. S. Cavaleiro, T. Torres, D. M. Guldi, *Org. Lett.* **2007**, 9, 1557; b) O. Trukhina, M. Rudolf, G. Bottari, T. Akasaka, L. Echegoyen, T. Torres, D. M. Guldi, *J. Am. Chem. Soc.* **2015**, 137, 12914; c) A. Hausmann, A. R. M. Soares, M. V. Martínez-Díaz, M. G. P. M. S. Neves, A. C. Tomé, J. A. S. Cavaleiro, T. Torres, D. M. Guldi, *Photochem. Photobiol. Sci.* **2010**, 9, 1027; d) L. M. O. Lourenço, A. Hausmann, C. Schubert, M. G. P. M. S. Neves, J. A. S. Cavaleiro, T. Torres, D. M. Guldi, J. P. C. Tomé, *ChemPlusChem* **2015**, 80, 832.
- [12] B. B. Berna, B. Platzer, M. Wolf, G. Lavarda, S. Nardis, P. Galloni, T. Torres, D. M. Guldi, R. Paolesse, *Chem. Eur. J.* **2020**, 26, 13451.
- [13] a) M. S. Rodríguez-Morgade, M. E. Plonska-Brzezinska, A. J. Athans, E. Carbonell, G. de Miguel, D. M. Guldi, L. Echegoyen, T. Torres, *J. Am. Chem. Soc.* **2009**, 131, 10484; b) M. Krug, C. Stangel, A. Zieleniewska, T. Clark, T. Torres, A. G. Coutsolelos, D. M. Guldi, *ChemPhysChem* **2019**, 20, 2806; c) G. Rotas, M. B. Thomas, R. Canton-Vitoria, F. D'Souza, N. Tagmatarchis, *Chem. Eur. J.* **2020**, 26, 6652; d) D. Badgurjar, S. Seetharaman, F. D'Souza, R. Chitta, *Chem. Eur. J.* **2021**, 27, 2184; e) N. Zarrabi, C. O. Obondi, G. N. Lim, S. Seetharaman, B. G. Boe, F. D'Souza, P. K. Poddutoori, *Nanoscale* **2018**, 10, 20723.
- [14] R. Orłowski, D. Gryko, D. T. Gryko, *Chem. Rev.* **2017**, 117, 3102.
- [15] J. K. Laha, S. Dhanalekshmi, M. Taniguchi, A. Ambroise, J. S. Lindsey, *Org. Process Res. Dev.* **2003**, 7, 799.
- [16] D. T. Gryko, K. E. Piechota, *J. Porphyrins Phthalocyanines* **2002**, 06, 81.
- [17] P. G. Seybold, M. Gouterman, *J. Mol. Spectrosc.* **1969**, 31, 1.

Manuscript received: October 28, 2021

Accepted manuscript online: January 27, 2022

Version of record online: February 10, 2022